This is a repository copy of *Foaming Behavior of Polymer-Coated Colloids: The Need for Thick Liquid Films*.

White Rose Research Online URL for this paper:
http://eprints.whiterose.ac.uk/120492/

Version: Accepted Version

Foaming behavior of polymer-coated colloids: the need for thick liquid films

Kai Yu[1], Huagui Zhang[1], Chris Hodges[1], Simon Biggs[2], Zhenghe Xu[3], Olivier J. Cayre[1], and David Harbottle[1*]

1 School of Chemical and Process Engineering, University of Leeds, UK
2 Faculty of Engineering, Architecture and Information Technology, The University of Queensland, Australia
3 Department of Chemical and Materials Engineering, University of Alberta, Canada

*Corresponding author
David Harbottle, E: d.harbottle@leeds.ac.uk ; T: +44 (0)113 343 4154

ABSTRACT

The current study examined the foaming behavior of poly(vinylpyrrolidone) (PVP)-silica composite nanoparticles. Individually, the two components, PVP and silica nanoparticles, exhibited very little potential to partition at the air-water interface and, as such stable foams could not be generated. In contrast, combining the two components to form silica-PVP core-shell nanocomposites led to good 'foamability' and long-term foam stability. Addition of an electrolyte (Na_2SO_4) was shown to have a marked effect on the foam stability. By varying the concentration of electrolyte between 0 and 0.55 M, three regions of foam stability were observed: rapid foam collapse at low electrolyte concentrations, delayed foam collapse at intermediate concentrations, and long-term stability (~ 10 days) at the highest electrolyte

concentration. The observed transitions in foam stability were better understood by studying the microstructure and physical and mechanical properties of the particle-laden interface. For rapidly collapsing foams the nanocomposite particles were weakly retained at the air-water interface. The interfaces in this case were characterized as being "liquid-like" and the foams collapsed within 100 min. At an intermediate electrolyte concentration (0.1 M), delayed foam collapse over ~16 h was observed. The particle-laden interface was shown to be pseudo solid-like as measured under shear and compression. The increased interfacial rigidity was attributed to adhesion between interpenetrating polymer layers. For the most stable foam (prepared in 0.55 M Na_2SO_4), the ratio of the viscoelastic moduli, G'/G" was found to be equal to ~ 3, confirming a strongly elastic interfacial layer. Using optical microscopy, enhanced foam stability was assessed and attributed to a change in the mechanism of foam collapse. Bubble-bubble coalescence was found to be significantly retarded by the aggregation of nanocomposite particles, with the long term destabilization being recognized to result from bubble coarsening. For rapidly destabilizing foams, the contribution from bubble-bubble coalescence was shown to be more significant.

KEYWORDS: foams, polymer-nanoparticle composites, air-water interface, bubble coarsening, bubble coalescence.

1. INTRODUCTION

Assembly of colloidal particles at fluid interfaces is a promising technique for synthesizing novel materials which can be potentially used in biomedicine, materials science, and formulated products.[1, 2, 3, 4, 5, 6] In many products, colloid particles and a wide range of chemical additives such as surfactants and polymers often co-exist to provide desirable properties, which usually

include immiscible fluids (liquid-liquid or gas-liquid). Upon mixing in these systems, interfaces generated are stabilized by the chemical additives. While the amphiphilicity of surfactants governs their interfacial activity, the surface chemical uniformity of a particle means that contrasting affinities for both the polar/non-polar fluids is not readily achieved, although the use of Janus particles is a route to provide such amphiphilicity.[7]

The potential for a particle to reside at an interface is influenced by the particle wettability, represented by the three phase contact angle (θ).[8] Previous studies showed that good emulsion stabilizing particles exhibit contact angles close to 90°. For foams, this critical contact angle is higher than 90°, with optimum stabilizing conditions reported for contact angles close to 120°.[9] Relatively small deviations away from this optimum contact angle can lead to dramatic changes in foam stability, with particles behaving as de-stabilizers rather than stabilizers. Various routes to modify particle wettability have been demonstrated, which include silanization,[8, 10] surfactant adsorption,[11] addition of electrolyte,[12] polymer grafting,[13, 14] surface roughness modification,[15] and more recently switching of physical conditions of the system such as temperature, pH, light, or CO_2 addition/removal.

For foams stabilized by surfactant, the behavior and mechanisms of foam collapse have recently been reviewed by Briceno-Ahumada and Langevin. They showed that the rate of bubble coarsening was proportional to the permeability of the interfacial layer, which was dependent on the layer thickness and the surfactant packing density, a factor that can be controlled by introducing surfactant mixtures.[16] The added benefit of using composite surfactant-particles to arrest bubble coarsening has been demonstrated in several recent studies.[11, 17, 18] Through the electrostatic attraction between cetyltrimethyl ammonium bromide (CTAB) and silica particles,

foams stabilized by composite particles were shown to exhibit substantially longer foam lifetimes than surfactant-only stabilized foams.[17] The enhanced foam stability was shown as a reduction in the rate of bubble coarsening once the particle concentration at the interface was sufficiently high to effectively "jam" the foam network.[17] The critical condition to minimize bubble coarsening was influenced by the particle number density at the interface, which was directly related to the surfactant concentration.[11, 18] During bubble coarsening, smaller bubbles were observed to reduce in size before the interface eventually buckled.[17] Interfacial buckling confirmed the strong retention of the surfactant-particle composites at the gas-liquid interface, with the energy for particle detachment affected by the wetting angle. The critical wetting angle has been shown to vary between 50° and 70°, depending on the surfactant concentration when below the critical micelle concentration (CMC).[18]

For an interface to buckle Erni et al.[19] confirmed that the two interfacial rheological contributions, shear and dilatational, should be non-zero, and the interface should behave as an elastic solid, i.e. G'(storage modulus) > G"(loss modulus). With continued bubble shrinking, the irreversibly adsorbed chemical species eventually 'jam' and resist any further surface area reduction, until a critical compressive strain is surpassed to buckle the interface. The ability for an interface to resist in-plane shear has recently been shown as a key contributing factor in stabilizing droplets. At the liquid-like state (G" > G') the interfacial layer provides little resistance to droplet-droplet coalescence. However, when the condition for interfacial buckling is satisfied and the interface is described as being solid-like, two interacting droplets do not coalesce.[20] The stabilizing mechanism is attributed to the interfacial shear yield stress which must be exceeded in order for the interfacial layer to flow away from the contact area and initiate

droplet coalescence. For foams stabilized by surfactant-only, the conservation of the surfactant surface coverage through the reversible adsorption of surfactant molecules mitigates the buckling.

Langevin and co-workers recently demonstrated that the shear rheology of a surfactant-particle-laden interface satisfies the soft glassy rheological response, with the elastic contribution of the layer being dependent on the surfactant concentration.[11] The data qualitatively verify previous observations of foam lifetime. However, the contribution of interfacial shear rheology to foam destabilization may be more relevant to bubble coalescence than bubble coarsening, as the arrest of bubble coarsening has frequently been discussed in terms of the dilatational elasticity.[16] For a single bubble, coarsening can be stopped if the elastic compression modulus E of the interfacial layer is at least twice the gas-liquid surface tension (γ). Following the derivation by Gibbs,[9, 10, 16] bubble coarsening ceases when the Laplace pressure approaches zero. While numerous practical foam studies have verified this criterion, contradictions have also been reported, which were often justified by the formation of multilayers.[10]

The application of polymers to stabilize foams has received little scientific attention due to weak adsorption of polymers at the gas-liquid interface.[21, 22] However, polymer-surfactant mixtures have been shown to extend the lifetime of thin liquid films by promoting the formation of surface complexes below the critical aggregation concentration (CAC). The presence of surface complexes leads to an increase in the surface viscosity and steric repulsion between two approaching fluid interfaces.[22, 23] Above the CAC the polymer-surfactant complexes gel, significantly increasing the bulk fluid viscosity and extending film lifetime. In this case the maximum foam stability was observed at the onset of surfactant-polymer precipitation.[23, 24]

More recently, emulsions and foams stabilized by polymer microgel particles have demonstrated tuneable functionality in two-phase systems by the use of thermal-responsive or pH-responsive polymers.[25, 26] The co-polymer ratio in microgel particles has been shown to affect the emulsifying potential of particles. Compared with rigid microgel particles, 'softer' and more responsive particles produce emulsions of extended lifetime.[27] Pseudo-microgel particles formed by grafting polymer onto the surface of nanoparticles have also been proven to be good emulsifying agents, stabilizing emulsions for several months. Tilton and co-workers reported that the best nanoparticles for emulsification had a low concentration of polymer chains adsorbed on their surface (0.077 chains/nm^2), stabilizing emulsions with only 0.05 wt% polymer-grafted nanoparticles. This concentration of particles is much lower than that usually required to stabilize Pickering emulsions.[13] Compared with hard spheres, core-shell particles were shown to be good foaming/emulsifying agents and stabilizers since they are capable of reducing the surface tension,[14] facilitate the adsorption of particles at the fluid-fluid interface,[14, 28, 29] and provide a route to control the particle-particle separation distance to adjust the structure and mechanical strength of interfacial layers.[30, 31, 32]

To the best of our knowledge, the foaming ability of polymer-particle composites formed via polymer physisorption has not been considered in detail, despite the fact that polymers such as PVP are commonly used as co-stabilizers in many food, pharmaceutical, cosmetic and detergent formulations.[21] PVP is widely used in formulation because of its good solubility in water and organic solvents, as well as its ability to strongly adhere on different materials via hydrogen bonds and acid-base interactions.[22, 33, 34] The simpler physisorption than chemical grafting of polymer on nanoparticles is advantageous, especially when mass manufacturing is required for

6

desired day-to-day applications. Polymers such as PVP adsorb at many sites per nanoparticle, and therefore are not likely to desorb once attached to the nanoparticle surface, which is also an important factor when removing excess surface active species prior to needed formulation.[35] In the current study, we focus on the interfacial properties of polymer-particle composites formed via polymer physisorption. The role of electrolyte concentration on the mechanical response of deposited particle layers was investigated and correlated to the observed transitions in foam stability.

2. MATERIALS AND EXPERIMENTAL METHODS

2.1 Materials. PVP with a molecular weight of 40 kDa was purchased from Alfa Aesar (UK) and used as received. Ludox AS40 silica nanoparticles were purchased from Sigma-Aldrich (UK) as a 40 wt% aqueous suspension. Prior to its use the silica particle suspension was diluted to 10 wt% using Milli-Q water and then ion exchanged using Amberlite IRN 50 resin (Alfa Aesar, UK) to remove excess SO_4^{2-} counter-ions. The removal of excess counter-ions was verified by conductivity measurements of the diluted suspensions (reduced from ~225 ± 30 µS/cm to ~53 ± 10 µS/cm). The particle hydrodynamic diameter was determined using a Malvern ZetaSizer Nano ZS (Malvern Instruments, UK) to be ~ 34 nm with a PDI of 0.14. Milli-Q water with a resistivity of 18.2 MΩ.cm was used throughout the study and sodium sulphate (99+%. A.C.S. R, Sigma Aldrich, UK) was used as received without further purification for changing the electrolyte concentration.

2.2 Preparation of PVP coated silica nanoparticles. To prepare the PVP coated silica nanoparticles, henceforth referred to as composite particles, 30 mL of 10 wt% silica

nanoparticle suspension was added dropwise to 5 wt% PVP solution (40 mL) under gentle agitation. The PVP-silica suspension was continually mixed for 12 h to ensure PVP adsorption. Excess or weakly adsorbed PVP was removed from the silica particle suspension by centrifuging the sample at 13,000 rpm for 4 h. The supernatant was removed using a wide bore pipette before re-dispersing the centrifuged particles in Milli-Q water using mild sonication. The wash process was repeated several times and complete removal of any unadsorbed PVP was verified by measuring the surface tension of the removed supernatant after each wash cycle. Complete PVP removal was assumed when $\gamma_{a/w}$ of the removed supernatant reached $\sim$ 72.3 mN/m, at 25 °C.

PVP adsorption on the silica nanoparticles was confirmed by transmission electron microscopy (TEM) (see Fig. S1b), and the amount of adsorbed PVP determined using thermo-gravimetric analysis (TGA) (Q-500- TA, USA). For this purpose, 5-10 mg of the composite particles was heated from 30°C to 900°C (the thermal degradation temperature of PVP is around 400 °C [36]) at a 10°C/min heat rate under N_2 flow (50 mL/min). Here, silica only, PVP only and the empty aluminum pan were used as reference samples measured at identical conditions. Since all the trapped water should have evaporated around 100°C, the remaining mass of the composite particles at 100°C was used as a starting value for the analysis. Assuming that the PVP and SiO_2 mass loss from the composite particles up to 600°C are 100% and 0%, respectively (see Fig. S1a), the mass of adsorbed PVP with respect to the mass of silica nanoparticles was determined using the following equation

$$\frac{W_{PVP}}{W_{SiO_2}} = \frac{(W_{total,100°C} - W_{total,600°C})}{W_{total,100°C} - (W_{total,100°C} - W_{total,600°C})} \tag{1}$$

where $W_{total,100°C}$ and $W_{total,600°C}$ are the remaining masses of the composite particles at 100°C and 600°C, respectively. W_{PVP} and W_{SiO_2} represent the mass of PVP and silica in the composite particles, respectively. Based on Eq. 1, the adsorbed amount (Γ) of PVP on the silica nanoparticles is given by

$$\Gamma = \frac{W_{PVP}}{S_{spe} \times W_{SiO_2}} \qquad (2)$$

where S_{spe} is the specific surface area of silica nanoparticles (~135 m²/g for Ludox AS40).

2.3 Foam studies. After several washes the composite particles were re-dispersed in Milli-Q water to 10 wt% (particle to suspension mass). The suspension was refrigerated during storage. For foam testing, 10 mL of 1 wt% composite particles was prepared in 40 mL glass vial to an appropriate electrolyte concentration (between 0 and 0.55 M Na_2SO_4). The composite particle suspension was gently agitated using a laboratory carousel before 1 min of vigorous handshaking to generate the foam. The foamability and foam stability were visually measured by tracking foam heights at regular time intervals.

More detailed analysis of the foam destabilization mechanism was undertaken by studying bubble-bubble interactions using an optical microscope (Olympus BX51). Immediately following foaming, a small volume sample of the stable foam was extracted using a flat edged capillary tube (CM Scientific Ltd, 0.5 × 5 mm). The capillary tube was positioned below the air-foam interface and the sample gently drawn into the capillary tube with minimal disturbance. The dimensions of the capillary tube were chosen to minimize the deformation (i.e. flattening) of the foam bubbles. To prevent foam drying, both ends of the capillary tube were sealed using

9

Parafilm M®, and the sealed sample left un-disturbed on the optical microscope stage. The bubble size distribution as a function of foam aging was determined by measuring the diameter of individual bubbles using ImageJ software. All foam stability experiments were conducted at T = 25°C.

2.4 Characterization of composite particles interfacial layer.

2.4.1 π-A Isotherms. Surface pressure–area (π – A) isotherms of deposited particle layers at the air-water interface were measured using a Langmuir trough (Biolin Scientific, Sweden), with a maximum trough area of 85 cm^2. Surface pressure was measured using a paper Wilhelmy balance of dimensions 10×30 mm (w × l). Prior to each measurement the Delrin trough and baffles were thoroughly cleaned using 2 wt% Decon solution and rinsed with excess Milli-Q water and acetone. Any contaminants residing at the air-aqueous interface were first removed by compressing the barriers to the minimum trough area (20 cm^2), before aspirating the liquid surface under gentle suction. The "cleanliness" of the air-aqueous interface was verified by subsequent compressional isotherms. The trough was considered clean when the maximum deviation of the surface pressure under the maximum compression was less than 0.3 mN/m. The prepared particles (uncoated or composite) were first dispersed in the spreading solvent (mixture of water and isopropanol alcohol at a 1:1 vol/vol ratio), to a concentration of 0.5 wt% (based on the total suspension mass). Spread at the air-aqueous interface was 40 µL of 0.5 wt% particle suspension, ensuring that droplets were evenly distributed across the trough area and added without disturbing the interface (i.e., no droplet splashing). To evaporate the spreading solvent, the interface was left undisturbed for 30 min prior to collecting the π-A isotherms. The surface pressure of the particle layer under compression was continuously measured as the interfacial

area was reduced from 76 cm^2 to 20 cm^2 at a speed of 5 cm^2/min. All the measurements were repeated in triplicate with the results demonstrating a good repeatability (surface pressures at equivalent areas within $\pm$ 5%).

2.4.2 Microstructure of particle layer. The micron-scale structure of the composite particles layer at the air-water interface was studied under several states of compression (low $\rightarrow$ high compression). Following the layer preparation using the method described above, the composite particles layer was compressed to the desired surface pressure and held at a constant pressure for 5 min. The particle layer was then transferred from the air-aqueous interface to molecularly smooth mica basal planes using the Langmuir-Blodgett (LB) deposition technique.[37] The freshly cleaved mica substrate (Agar SCIENTIFIC, UK) was withdrawn through the air-aqueous interface at 90 mm/min whilst maintaining the surface pressure to ensure that the transfer ratio (deposited area to compressed area) remained constant at ~ 1. The deposited particle layers were carefully dried at slightly elevated temperature to minimize any drying effects, and stored in a ZONESEM sample cleaner before imaging using a scanning electron microscope (Hitachi SU8230, UK).

2.4.3 Interfacial Shear Rheology. The shear viscoelasticity of the composite particles interfacial layer was studied using a stress-controlled Discovery Hybrid Rheometer (DHR-2, TA Instruments, UK) equipped with a double wall ring (DWR) geometry.[38] To ensure a maximum measurement sensitivity the rheometer was calibrated using precision mapping with the transducer bearing mode set to soft. For the interfacial shear rheology measurements, 19.2 mL of the electrolyte solution was pipetted into the circular Delrin trough to ensure that the air-aqueous interface was pinned at the inner ridge of the trough. Spread at the air-aqueous interface was 10

µL of the composite particle suspension of 0.5 wt% solid content in a mixture of water/IPA (1:1 v/v). Prior to each measurement the DWR geometry was cleaned in acetone and washed with excess Milli-Q water and then flamed to remove any organic contaminants. With the particle layer formed at the air-aqueous interface, and the spreading solvent being evaporated (evaporation time ~ 30 min), the DWR geometry was gently lowered and positioned to pin the air-aqueous interface. Once positioned, the viscoelasticity of the interfacial layer was determined from data collected whilst oscillating the DWR geometry at a constant frequency of 0.5 rad/s and varying strain between 10^{-2} % and 10^3 %. All the measurements were conducted at a constant temperature of 25°C. More details describing the experimental technique and procedures can be found elsewhere.[20, 28, 38]

2.4.4 Adhesion force measurements between two PVP coated surfaces using colloid probe technique. A Bioscope II AFM (Bruker, USA) was used to measure the interaction forces between two PVP coated surfaces using the colloid probe technique. The tipless silicon nitride cantilever (DNP-020, Bruker AFM Probes International Inc., USA), with a spring constant of 0.6 N/m determined by the thermal resonance method, was used to create colloid probes. Silica particles (Sigma Aldrich, UK) between 9 and 13 µm were attached to the cantilevers using a two-part epoxy glue (Araldite 2012) which was allowed to cure overnight. These probes were then examined by SEM (Hitachi TM3030, UK) to ensure that the particle was well centred and cleanly attached to the cantilever (see Fig. S2). A 1 cm^2 piece of silicon wafer (University Wafer Inc., Boston, USA) with a 100 nm top layer of silicon dioxide was placed into a UV/Ozone cleaner (Bioforce Nanosciences, Iowa, USA) for 30 min and then rinsed with Milli-Q water. Both the silicon wafer and the colloid probe were dipped into two trays each containing 10 ppm

40 kDa PVP for 10 min, after which the silicon wafer was rinsed with Milli-Q water and the colloid probe was dipped into a tray of Milli-Q water. Optical reflectometry data confirmed rapid adsorption of PVP on silica, reaching steady state conditions within 10 min (data not shown).

Force curves were obtained immediately after the PVP surface preparation to ensure that both PVP surfaces remained fully hydrated. Two or three drops of liquid (either Milli-Q water or Na_2SO_4 solution) were deposited onto the PVP coated wafer surface before immersing the colloid probe into this solution. All force curves were collected at 0.5 Hz at a minimum of 3 different surface sites. A minimum of 10 force curves per area were obtained

3. RESULTS AND DISCUSSION

3.1 Characterization of composite particles. PVP coverage on the silica nanoparticles was confirmed by TGA studies (see Fig. S1a). The resulting PVP surface coverage (Γ) was found to be ~ 0.9 mg/m^2, correlating well with previously published data obtained using depletion methods.[33, 35, 39] Using dynamic light scattering, the mean hydrodynamic diameter of the composite particles was found to be ~ 52 nm, confirming an approximate hydrated polymer shell thickness of ~ 9 nm. The core-shell structure of the composite particles is clearly visible in the TEM images shown in Fig. S1b with the thickness of the dried polymer shell being ~3-5 nm (images were analyzed using ImageJ).

The effect of electrolyte concentration on the stability of the composite particles was studied prior to assessing the particles foaming potential. Fig. 1 shows the dependence of the particle electrophoretic mobility and the mean particle size on the electrolyte concentration (0 to 0.1 M

Na$_2$SO$_4$). At low electrolyte concentrations the particle electrophoretic mobility was relatively high (~ -2.0 cm^2/Vs) with particles sizes in the range of 47 – 52 nm. The particles can therefore be considered as non-interacting and dispersed. The observed decrease in the measured particle size between water and 0.01 M Na$_2$SO$_4$ resulted from the change in the polymer conformation, shrinking back to the particle surface as the solvency of the polymer reduced in the divalent electrolyte solution. At 0.1 M electrolyte concentration the composite particles electrophoretic mobility decreased and the mean particle size increased. The onset of particle aggregation at 0.1 M was confirmed, with particle aggregation more pronounced with increasing electrolyte concentration. At the highest electrolyte concentration (0.55 M), the particle/aggregate size could not be accurately measured using the Nano ZS instrument due to sedimentation of the formed aggregates.
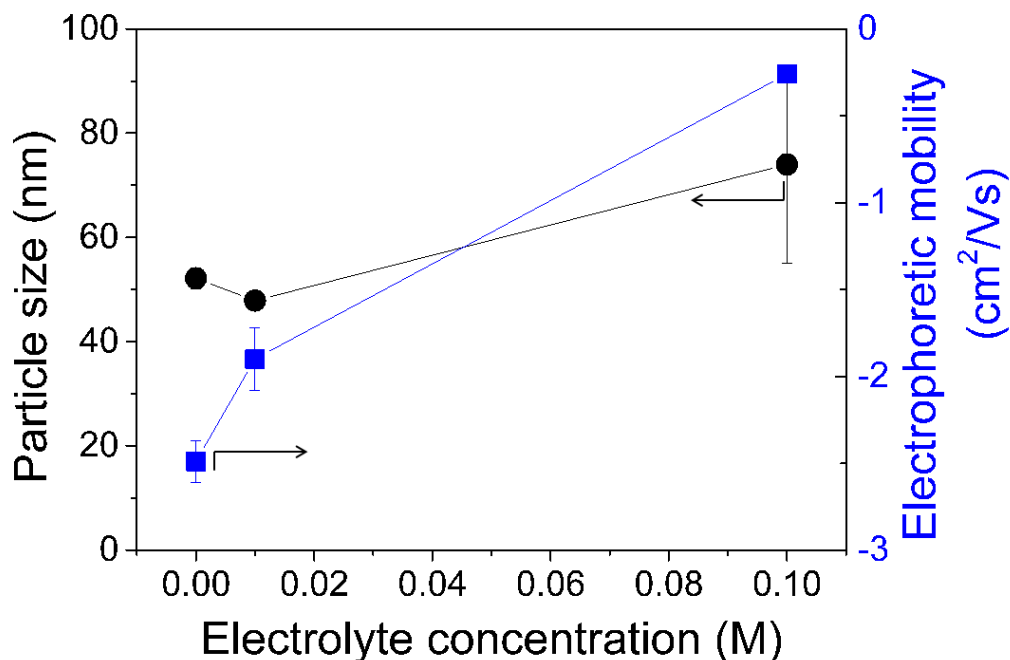
Figure 1. Measured hydrodynamic diameter of composite particles (symbol: circle), and particle electrophoretic mobility (symbol: square) as a function of the electrolyte concentration. Lines to guide the eye.

3.2 Foamability and foam stability. For particles to act as foaming agents they must demonstrate the ability to partition from the solvent and reside at the air-water interface. The particle desorption energy from an interface has been extensively discussed,[8, 11, 40, 41] with the desorption energy (W_r) given as a function of the air-water interfacial tension ($\gamma_{a/w}$), the particle radius (R), and the particle wettability which is described by the three-phase contact angle (θ). Increased foam stability in the presence of Brownian-like particles can be achieved by enhancing particle aggregation at the air-water interface, as shown in our recent publication,[40] increasing the particle wettability, or both. While increasing the electrolyte concentration enhances particle aggregation, measuring changes in the particle contact angle at an air-water interface can be challenging. However, a useful approximation can be made by measuring the three-phase contact angle of a sessile droplet on a PVP coated silica substrate.[12, 42] Fig. S3a in the Supporting Information confirms that increasing the electrolyte concentration from 0 to 0.55 M Na_2SO_4 increased slightly the three-phase contact angle from 23° to 39°. A slight increase in the three-phase contact angle, coupled with an increase in the aggregate size (with increasing electrolyte concentration) will ultimately improve particle retention at the air-aqueous interface.
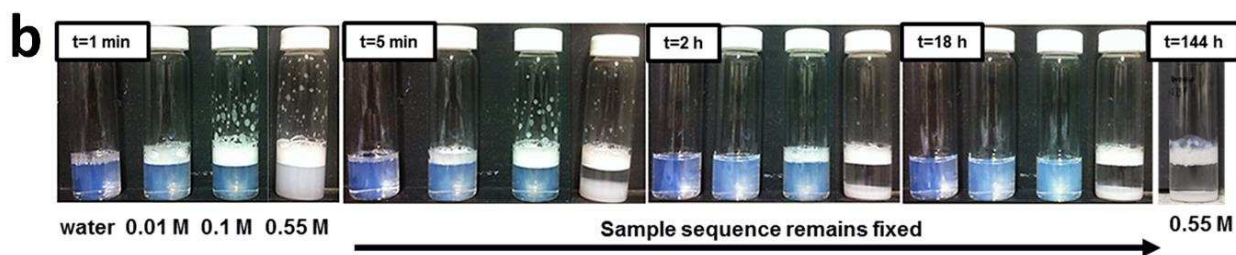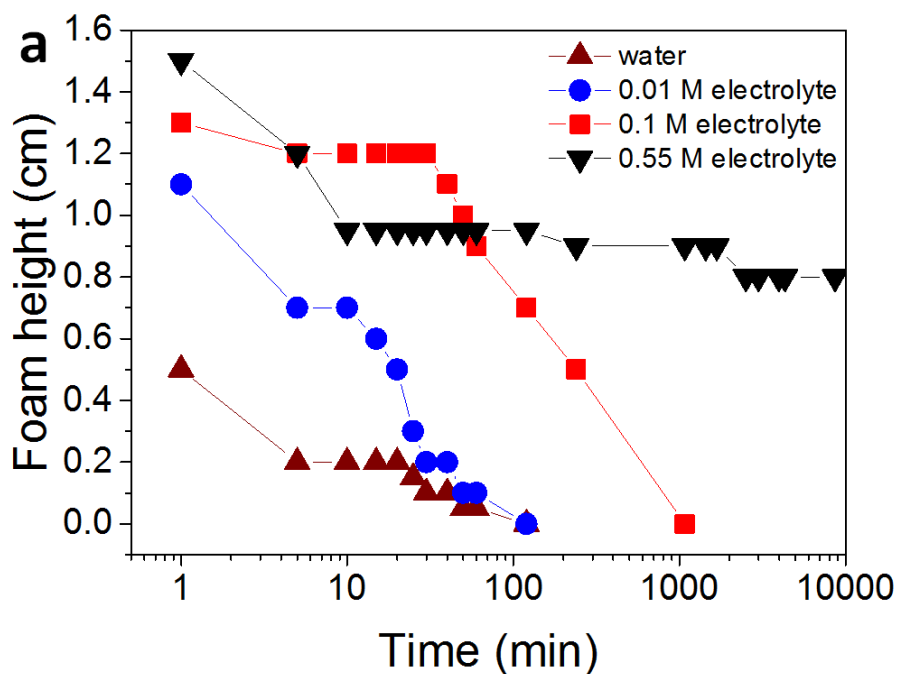
15

Figure 2. (a) Time-dependent stability of foams prepared using composite particles as a function of the electrolyte concentration (lines to guide the eye); (b) Images showing changes in foam height with aging time. The electrolyte concentrations are shown below each glass vial depicted at t = 1 min. Height of glass vial = 9 cm.

Foams were prepared using three potential foaming agents i) PVP, ii) hydrophilic silica nanoparticles and iii) composite particles, in four liquid environments of increasing electrolyte concentration. As expected, for the untreated hydrophilic silica nanoparticles, no foaming was observed and this was attributed to poor interfacial partitioning. Compared with hydrophilic silica nanoparticles, PVP exhibited greater surface activity reducing the air-aqueous surface

tension to ~ 61 mN/m at the highest electrolyte concentration (see Fig. S3b). Upon shaking, foams were readily formed confirming good 'foamability', but the foams rapidly collapsed within a few seconds once the shaking had ceased. Poor foam stability in the presence of polymers has been widely reported with rapid foam collapse being attributed to the low elasticity and viscosity of the interfacial layer.[43, 44]

Using composite particles as the foaming agent, the effect of electrolyte concentration was shown to have a marked effect on the foam stability. At all electrolyte concentrations the composite particles exhibited good foaming potential. However, the rate of foam collapse was shown to be sensitive to the electrolyte concentration. In the absence of any electrolyte the initial foam height was substantially less than foams formed in the presence of electrolyte. At low electrolyte concentrations ($\leq$ 0.01 M) the foams were observed to steadily collapse, with the foam height diminishing completely within 1 h. At intermediate electrolyte concentration (0.1 M) the foam collapse trend appeared different from the steady foam collapse observed at lower electrolyte concentrations. At 0.1 M, immediately following shaking (< 5 min), the foam height reduced by ~ 8% and then remained constant for the next 30 min. Subsequent collapse of the foam over the next 18 h followed an exponential decay, a typical decay profile for collapsing foams.[45, 46, 47] At the highest electrolyte concentration (0.55 M) partial foam collapse was observed immediately following shaking (< 10 min), most likely associated with liquid drainage from the foam.[47] However, unlike all other foams which eventually collapsed within several hours, the foam remained stable over a prolonged period of time. Fig. 2a shows a gradual reduction in the foam height (~ 15%) over a period of six days, with complete foam collapse observed after two weeks (data point not shown). These simple experiments highlight the

importance of solvent composition on the 'foamability' and stability of foams stabilized by composite particles. However, the mechanism that governs foam stability is not readily apparent.

The liquid volume fraction in the foams has been estimated by measuring the changes in both the liquid (V_{L1}-V_{L2}) and foam (V_F) volumes with aging time. Fig. S4 of the Supporting Information confirms that the 0.55 M foam remains considerably water-wet, with a liquid volume fraction of ~45 vol% after 6 days aging. High water retention in foams prepared using strongly aggregating particles is in good agreement with previously reported data.[48, 49] The water-wet foam (0.5 M) is in contrast to the 0.1 M Na_2SO_4 foam, which during aging gradually de-watered leading to a relatively dry foam (~15 vol% water) after 2 h aging.

Fig. 2b shows the general appearance of the foams and composite particle suspensions used in the foaming experiments. At low electrolyte concentrations ($\leq$ 0.1 M) a blue haze was observed in the aqueous sub-phase below the foam surface, thus confirming good dispersion of the composite particles. In contrast, the aqueous sub-phase containing 0.55 M electrolyte appeared white, resulting from increased scattering of visible light by the larger aggregates, which eventually settled to form a sediment bed on the base of the glass vial. These visual observations were in good agreement with the particle size data shown in Fig. 1.

3.3 Interfacial π–A isotherms and particle layer relaxation. To better understand the observed transitions in foam stability: rapid collapse, delayed collapse and long-term stability, the compressional and relaxation properties of the deposited composite particle layers were studied using an air-liquid Langmuir trough. Fig. 3 compares the π – A isotherms for all particle systems used in the current study. As expected, hydrophilic silica nanoparticles provided no resistance to lateral compression, depositing into the water. As a result, the surface

18

pressure remained extremely low (~ 0 mN/m) over the full compression range. When the composite particles were spread at the air-water interface the surface pressure at maximum compression increased to 2.8 mN/m, although exhibited little resistance to compression. It was evident that the presence of PVP improved particle retention at the air-water interface. Spreading a fixed volume of the composite particles on to a sub-phase of increasing electrolyte concentration (0.01 M, 0.1 M and 0.55 M), resulted in a progressive increase in the maximum measurable surface pressure, thus confirming the electrolyte concentration effect previously described. The effect of electrolyte concentration on particle retention at the air-aqueous interface was clearly evident at the maximum trough area (low compression), where the surface pressure of the particle layer increased from 0.4 mN/m to 2.0 mN/m when deposited on water and 0.55 M electrolyte solution, respectively.
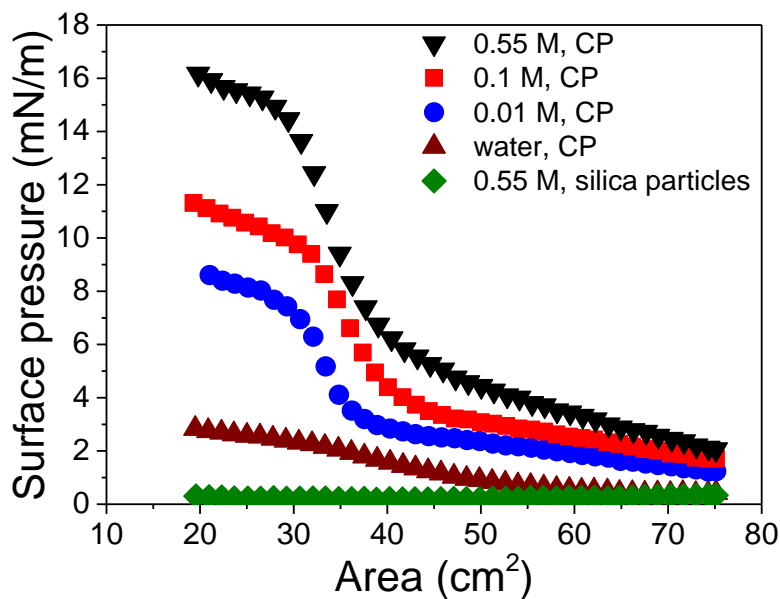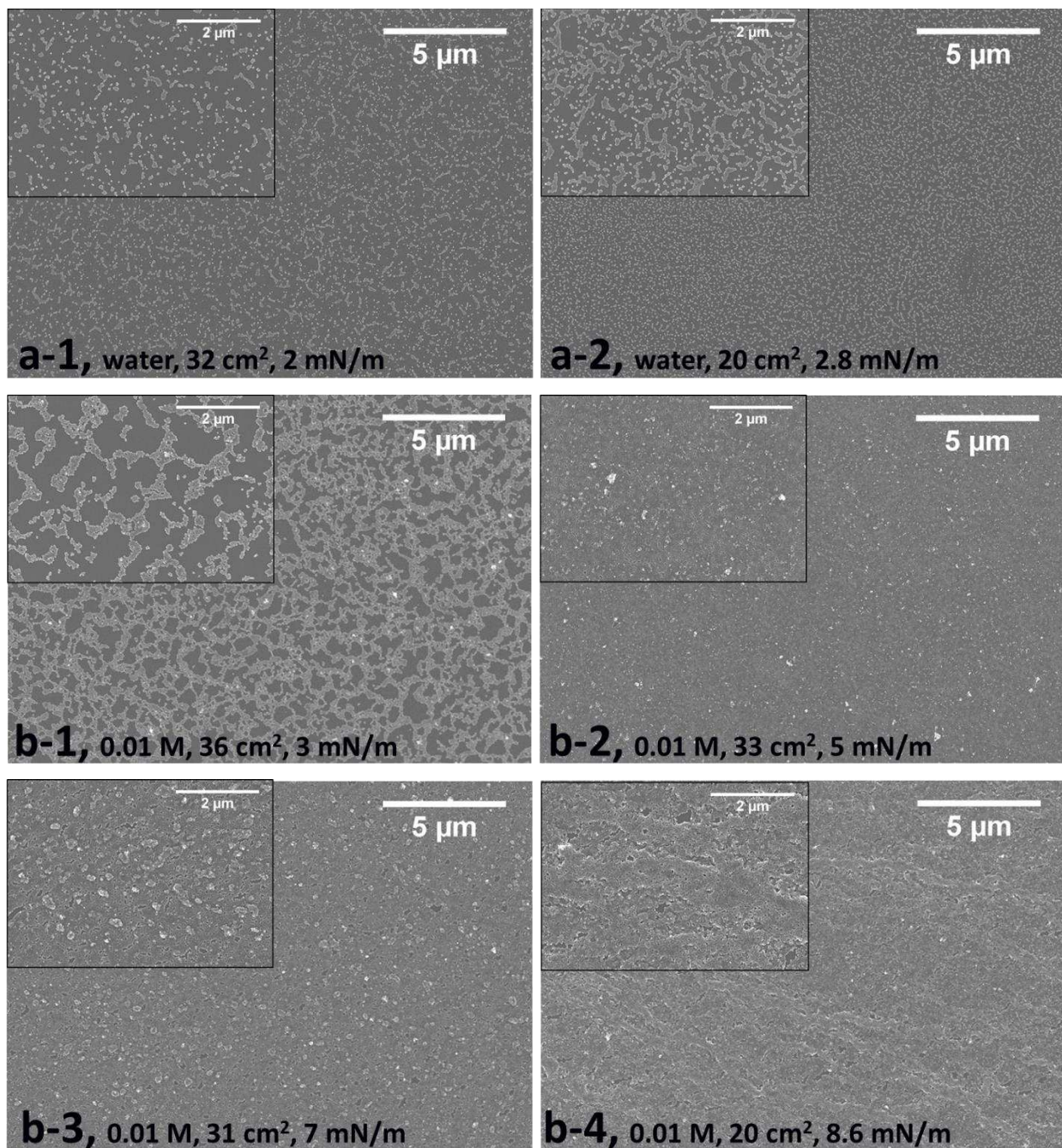
Figure 3. $\pi - A$ isotherms for silica and composite particles spread at the air-aqueous interface. The particle concentration and spreading volume were fixed at 0.5 wt% and 40 μL, respectively. (CP = composite particles).

The composite particles network was assessed by scanning electron microscopy (SEM) close to the gas-to-liquid (G-L) and liquid-to-solid (L-S) transitions, as well as the maximum interfacial layer compression (minimum trough area). The particle layers were recovered from the air-aqueous interface using the LB deposition technique (see Section 2). With no electrolyte addition the surface pressure of the composite particle layer remained low, and the corresponding SEM images (Fig. 4a-1) confirmed a lack of particle networking and the absence of a close-packed particle monolayer at the minimum trough area (Fig. 4a-2). At 0.01 M Na_2SO_4, the deposited particle layer was more interconnected but showed significant voids at the G-L transition (see Fig. 4b-1). With further compression ($\pi = 5\ mN/m$) the void domain size decreased to form an almost complete particle monolayer (Fig. 4b-2). Close to the L-S transition ($\pi = 7\ mN/m$), the particle network became sufficiently compressed that particle aggregates were displaced and formed a patchy multi-layer network (displaced particles identified as bright spots in the particle layer, see inset Fig. 4b-3). At maximum compression ($\pi = 8.6\ mN/m$), substantial displacement of particles resulted in the formation of a multi-layer network, with the second particle layer showing finger-like structures (see Fig. 4b-4). At 0.1 M Na_2SO_4, the surface pressures of the particle layer at equivalent trough areas (32 cm^2 and 20 cm^2) were approximately 40% higher than that at 0.01 M Na_2SO_4 electrolyte concentration. A multi-layer particle network was once again observed near the L-S transition (see Fig. 4c-1). However, under maximum compression substantial crumpling of the particle layer was observed, confirming buckling of the interfacial

particle layer under high lateral compression force (see Fig. 4c-2). An attempt was made to repeat the deposition and imaging protocol for the highest electrolyte concentration (0.55 M), however, significant salting on the mica substrate interfered with the sample imaging.
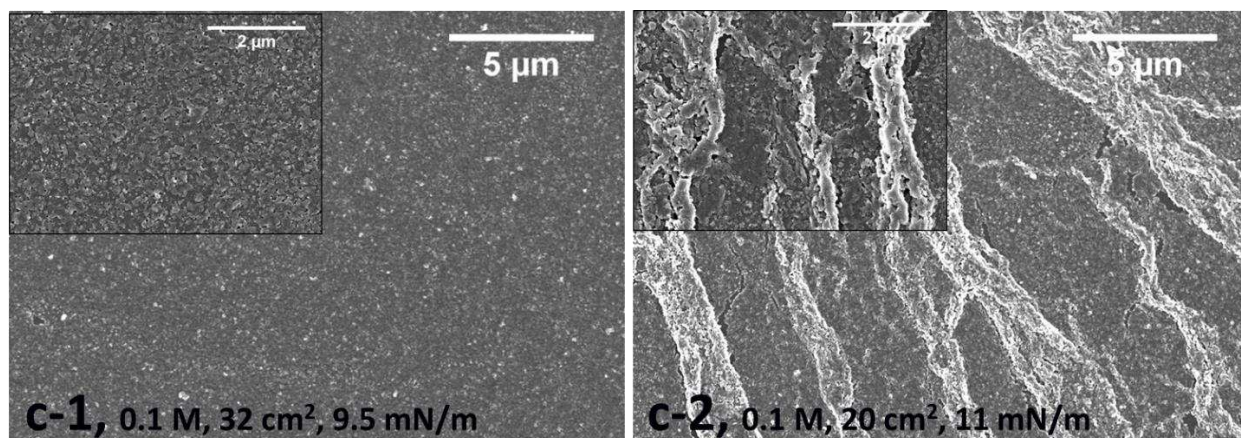
Figure 4. SEM images showing the surface pressure dependent micron-scale structure of deposited composite particle layers transferred from the air-aqueous interface. Sub-phase electrolyte concentration equal to 0 M, 0.01 M, and 0.1 M, as labelled. Trough area and film surface pressure provided for each micrograph.
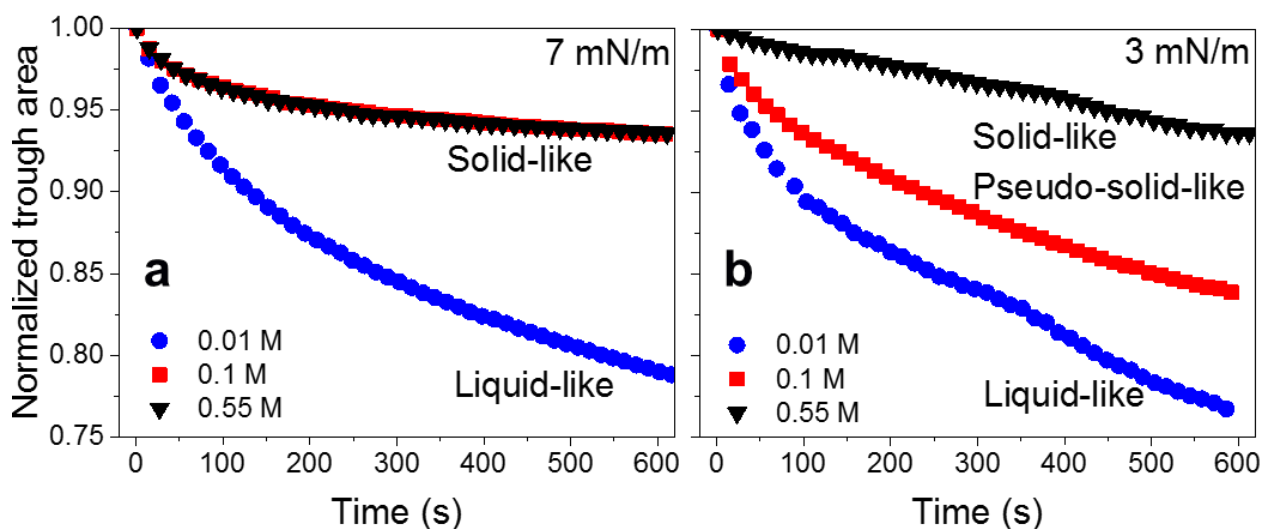

Figure 5. Relaxation/reorganization of particle layers compressed to a constant surface pressure of (a) 7 mN/m and (b) 3 mN/m.

Relaxation/reorganization of the composite particle layers at the air-aqueous interface was studied at constant surface pressures, 3 mN/m and 7 mN/m. A constant surface pressure

22

experiment was conducted to elucidate the mobility of the particle layers as a function of the sub-phase electrolyte concentration under equivalent compressional force, albeit the compression areas were slightly different. Firstly, a surface pressure of 7 mN/m was chosen to ensure that the particle layers were initially in the "liquid-phase" between the G-L and L-S transitions. With the target surface pressure reached, the barriers of the Langmuir trough were operated in feedback mode to ensure that the surface pressure remained fixed, and the trough area recorded over 600 s. Fig. 5a shows the time-dependent changes in the normalized trough area required to maintain a constant surface pressure. The trough area was normalized by the starting trough area which was a function of the sub-phase electrolyte concentration: 0.01 M = 32 cm^2, 0.1 M = 36 cm^2, and 0.55 M = 38 cm^2.

Quite interestingly there was a distinct division in the behaviour of the particle layers with the response clearly dependent on the sub-phase electrolyte concentration. At 0.01 M the trough area was shown to continually decrease such that the surface pressure of the composite particle-laden film could be maintained. This behaviour was characteristic of a liquid-like system where neighbouring particles are able to reorganize to an apparent lower energy state when under an applied load. At 600 s the trough area had reduced by 22%. At higher electrolyte concentrations (0.1 M and 0.55 M) the response was more solid-like, with only a 6% reduction in the trough area after 600s. The time-dependent response would indicate that following compression the interfacial particle layer was effectively "locked in place" and could not reorganize under lateral compression to alleviate the applied pressure.

At a lower surface pressure, 3 mN/m (Fig. 5b), ensuring that all three particle layers were in the "gas-phase", the time-dependent response of the particle layers differed only slightly. For the

case of 0.01 M and 0.55 M electrolyte solution, the response of the compressed particle layers showed similar behaviors to those observed at higher surface pressure, i.e. liquid-like and solid-like states. However, for the 0.1 M electrolyte solution the particle layer showed a different time-dependent response, as shown by the continued reduction in the trough area to maintain the constant surface pressure (3 mN/m). Since the response was between the two extremes (liquid-like and solid-like states), we have termed this particle layer to be "pseudo solid-like" at low surface pressure.

A multi-compression isotherm (first and second cycle) was conducted to examine the influence of composite particle desorption under compression. Fig. S6 of the Supporting Information showed little difference between the first and second compression cycles, with the two isotherms overlapping when the surface pressure was between 1.75 mN/m and 2.25 mN/m. The small differences between the consecutive isotherms (at low surface pressures) may indicate an effect of composite particle desorption, although this effect is not thought to be a contributing factor to the time-dependent changes shown in Fig. 5.

3.4 Interfacial rheology of deposited particle layers. Interfacial mobility of the particle layers was measured using the interfacial DWR geometry. Recent studies have highlighted the importance of interfacial shear elasticity to stabilize liquid droplets.[14, 20, 27, 50] For strongly elastic interfacial layers the shear strength is a major contributing factor inhibiting droplet coalescence. If the applied load is sufficient to exceed the shear yield stress, the interfacial layer will rupture to cause droplet coalescence. It is important to note that the shear interfacial viscoelasticity correlates to the likelihood of droplet coalescence but has not been

considered in terms of hindrance to droplet coarsening. Droplet coarsening is frequently correlated to the dilatational elasticity.[10, 16]

To replicate the condition of low surface pressure (equivalent to the particle surface coverage at the maximum Langmuir trough area), the spreading volume was adjusted in such a way that the expected surface pressure for the interfacial shear rheology measurements was in the region of 3 mN/m. Following particle deposition, the viscoelasticity of the composite particle layers was measured at constant oscillation frequency of 0.5 rad/s and increasing strain between 10^{-2} % and 10^3 %.

The open and closed symbols in Fig. 6 represent the elastic (G') and viscous (G'') contributions, respectively. When oscillating in the linear viscoelastic region, at the lowest electrolyte concentration (0.01 M) the viscoelastic moduli (G' and G'') are almost equal (2.7 to 5.9×10^{-5} N/m). The rheology of the deposited particle layer can therefore be described as "weakly elastic". At 0.1 M Na_2SO_4, the viscoelasticity of the particle layer increased, exhibiting a higher elasticity with G' = 2.2×10^{-3} N/m and the G'/G'' ratio equal to ~ 3. The viscous to elastic ratio remained unchanged at the highest electrolyte concentration (0.55 M), although the elasticity of the particle layer increased by almost an order of magnitude as compared with the case of 0.1 M. This substantial increase in elasticity of the particle layer was in good agreement with the relaxation data shown in Fig. 5b, and supports the general observation of a more rigid interfacial particle layer at higher electrolyte concentrations.

With increasing oscillation strain the linear viscoelastic region was exceeded as the mechanical structure of the composite particle layer fractured under larger deformations. Increasing the oscillation strain led to a reduction in both the G' and G'' contributions as the particle aggregates

25

begin to flow. Eventually a critical strain is surpassed when the film transitions from solid-like (G' > G") to liquid-like (G' < G") response.[20, 27] In an oscillation stress ramp test (data not shown) the yield point (τ_y) of the three particle layers, identified as the crossover in G' and G" (i.e. G" = G'), was observed to increase from 4.3×10^{-6} N/m to, 2.4×10^{-5} N/m and 5.9×10^{-5} N/m with increasing Na_2SO_4 concentration from 0.01 M to 0.1 M and 0.55 M, respectively.

Figure 6. Strain dependent viscoelasticity of the composite particle layers spread at the air-aqueous interface. Sub-phase electrolyte concentration: 0.01 M, 0.1 M and 0.55 M Na_2SO_4; particle spreading concentration = 0.5 wt%; spreading volume = 10 μL.

3.5 Interaction forces between PVP coated surfaces. The influence of electrolyte concentration on the interactions between PVP polymer coated silica surfaces was investigated using the AFM colloid probe technique. Fig. 7 shows the results of interaction forces as two PVP

coated surfaces approach each other in aqueous electrolyte solutions. In 0.01 M Na$_2$SO$_4$ solution, the forces are monotonically repulsive, with the long-range interaction taking the form of an exponential decay. Although only the first few nm of the observed repulsion (i.e. from 40 to approximately 30 nm) is anticipated from the electrostatic component of the interaction, since the Debye length is only ~ 1.8 nm for 0.01 M divalent electrolyte solution, this repulsion was sufficiently strong that it was detected at separations of 2 or 3 times the Debye length.[51] At separations closer than 30 nm the measured repulsive force was from direct chain-chain interactions (steric forces). Gentle compression of these layers under the applied force of the AFM cantilever was measured with no obvious overlapping, indicating a soft layer on silica surfaces. Steric repulsion between the two interacting polymer layers can be pseudo-quantitatively described by the Alexander-de Gennes (AdG) theory. When two polymer brush layers approach each other, a critical distance is eventually reached when the loops and tails of the polymer overlap, leading to an increase in the local density of "polymer segments". The resulting polymer overlap leads to an increase in osmotic pressure and repulsive interaction energy. Applying the Derjaguin approximation, the total interaction force is given by [52]

$$\frac{F(D)}{R} = \frac{16\pi kTL}{35s^3}\left[7\left(\frac{2L}{D}\right)^{5/4} + 5\left(\frac{D}{2L}\right)^{7/4} - 12\right] \qquad (3)$$

where k is the Boltzmann constant, T is the temperature, D is the surface separation distance, s is the mean distance between anchoring sites on the surface, and L is the uncompressed brush layer thickness. Since the absolute surface separation distance is unknown, the fully compressed layer thickness was estimated and used to offset the data. The AdG model fitting for interacting PVP polymer surfaces in 0.01 M Na$_2$SO$_4$ is shown in Fig. 7b. The fitting parameters s and L are 1.69

nm and 31 nm, respectively. With the uncompressed brush layer thickness exceeding the room temperature R_G for 40 kDa PVP (R_G = 7 nm), the likely configuration for the PVP polymer is consistent with a high adsorption density, and the polymer brush extending slightly into solution beyond a compact PVP layer.
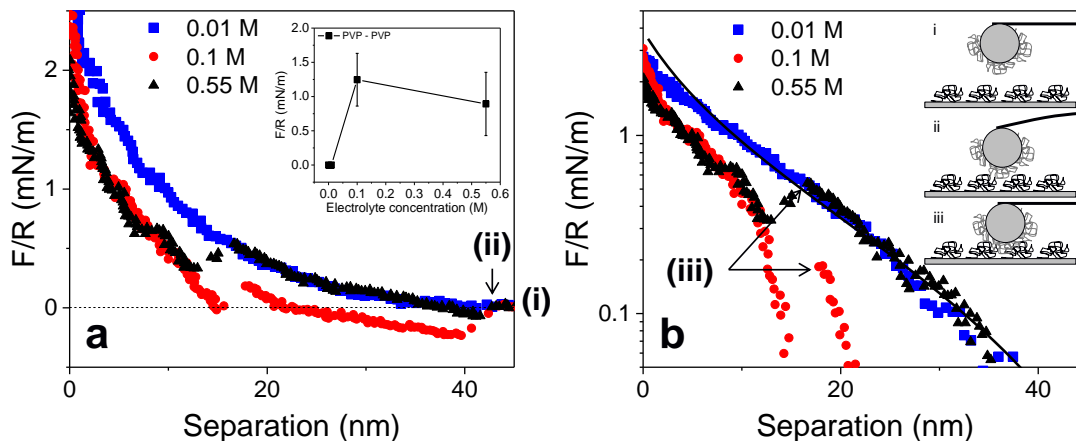

Figure 7. AFM force curves showing the influence of Na_2SO_4 concentration on the interactions between two approaching PVP coated silica surfaces using the colloid probe method. a) Approach force curves shown on a linear scale; inset shows the adhesion data obtained between PVP polymer coated silica surfaces. b) Approach force curves shown on a semi-log scale including the AdG theory (solid line) with fitting parameters s = 1.69 nm and L = 31 nm; inset highlighting the likely interactions between the approaching polymer layers in a poor solvent. i) out of contact, ii) jump-in due to intersegment attraction, iii) push-through associated with the fusion of polymer layers.

For the force curves obtained in 0.1 M and 0.55 M Na_2SO_4 aqueous solutions, we expect minimal electrostatic interactions due to significant compression of electrical double layers. Instead, a jump of the colloid probe towards the surface was observed at separation distances

equal to 40 nm, followed by a second jump at distances less than 20 nm under further compression. The measured jump-in at long range was attributed to intersegment attraction between the outermost polymer segments. The fact that the observed interaction force for the two PVP surfaces interacting at ~ 40 nm was weakly attractive suggests that aggregation of composite particles under these conditions should be favoured. The second jump-in is thought to be associated with a push-through event and fusion of the opposing polymer layers, see schematic in Fig. 7b.

The inset in Fig. 7a shows that no adhesion was measured between PVP coated surfaces in 0.01 M Na_2SO_4. Weak adhesion of the polymer coated surfaces was only measured at higher electrolyte concentrations, with similar values being recorded for both 0.1 M and 0.55 M Na_2SO_4. The measured adhesion can be attributed to interpenetration and attraction between polymer segments on opposing surfaces.

3.6 Optical microscopy. Following liquid drainage, foam destabilization was attributed to either bubble coalescence and/or bubble coarsening (i.e. Ostwald ripening driven by a gradient of Laplace pressures). To better understand the governing mechanism for foam collapse, as shown in Fig. 2a, an optical microscope study was conducted focusing on a few foam bubbles. Fig. 8a shows the bubble size distributions determined by analysing a sequence of images using ImageJ software. To ensure reasonable statistical certainty each bubble size distribution was determined from analysing a minimum of 20 bubbles.

Unfortunately, foam bubbles generated in 0.01 M electrolyte solution collapsed during foam transfer and could not be analysed, thus confirming the fragility of the particle-laden interface. For 0.1 M Na_2SO_4 foam, the number of bubbles within the glass capillary was observed to

decrease during the 230-min aging time, which corresponded to an increase in the average bubble size and a broadening of the bubble size distribution (indicated by the "error" bars in Fig. 8a). An increase in bubble size and polydispersity was also evidenced in the images taken at 1, 29 and 72 min aging, see Fig. S7 of the Supporting Information. While it was difficult to determine the dominant mechanism for bubble growth, bubble-bubble coalescence was clearly observed in the 0.1 M Na_2SO_4 foam (Fig. 8b.), as evidenced by the periodic 'jumps' in the bubble size, thus suggesting the occurrence of bubble coalescence leading to rapid bubble growth (Fig. 8a., symbols: open circles).
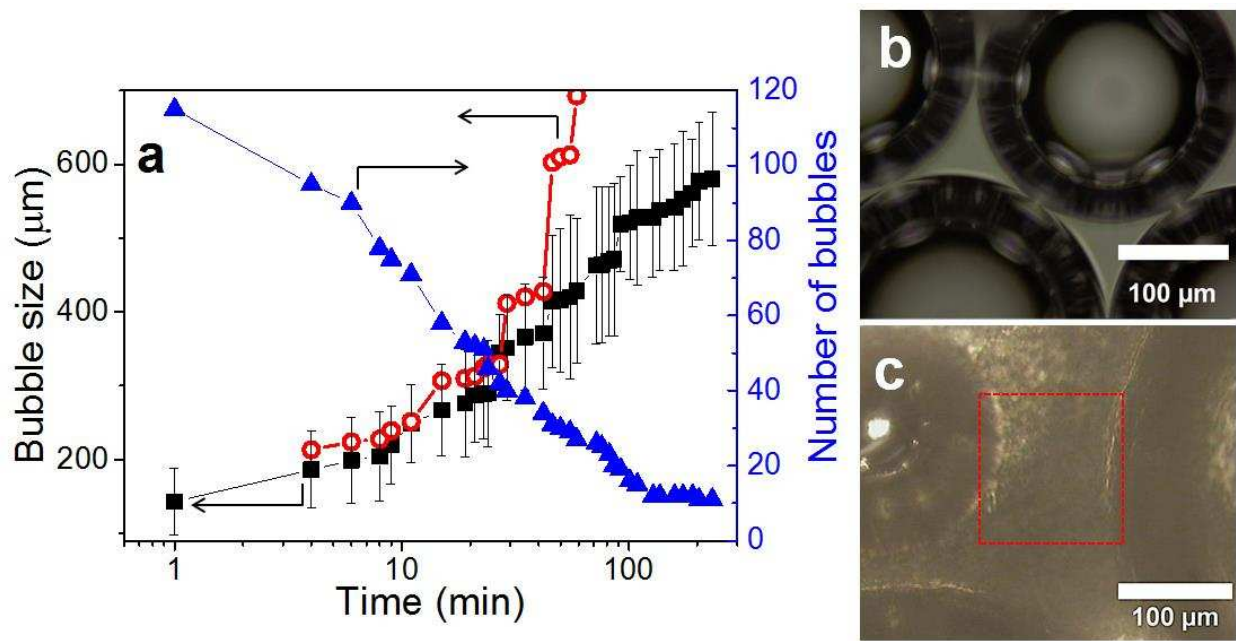

Figure 8. (a) Average bubble size (symbol: closed squares) and number of bubbles (symbol: closed triangles) as a function of the foam aging time. Open symbols (circle) correspond to the time-dependent growth of a typical bubble (electrolyte concentration = 0.1 M Na_2SO_4). Optical microscope images of fresh foam bubbles dispersed in (b) 0.1 M Na_2SO_4 and (c) 0.55 M Na_2SO_4.

Fig. 9 shows a sequence of images which depict the time-dependent shrinkage of an isolated bubble in the 0.55 M Na_2SO_4 foam. At t = 1 min the bubble size was approximately 100 μm before decreasing in size and eventually disappearing below the resolution of the optical microscope at t = 45 min. As the bubble size reduced the particle layer was observed to detach from the air-aqueous interface, forming a crumpled particle layer on the surface of the glass capillary. This finding confirmed that the particle layer was only weakly attached at the air-aqueous interface, and was not able to resist bubble coarsening. Since bubble coalescence was not observed during foam aging, the dominant mechanism for foam collapse was anticipated to be bubble coarsening. Hence, while bubble coarsening was expected to occur in all foam systems, the extent of droplet coalescence has been demonstrated to reduce with increasing electrolyte concentration.
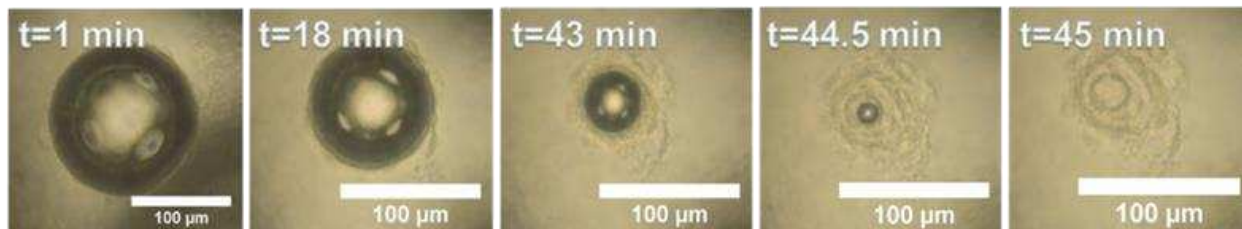

Figure 9. Optical microscope images of an isolated bubble aging in 0.55 M electrolyte solution.

To verify bubble coarsening in the 0.55 M Na_2SO_4 foam, the time-dependent sizes of several small (< 300 μm) and several large (> 700 μm) bubbles were measured. For the large bubbles shown in Fig. 10b, the bubble sizes increased slightly over the duration of the measurement (ca. 500 min). This was in contrast to the smaller bubbles shown in Fig. 10a, which were observed to decrease in size and eventually disappear. The time for complete bubble disappearance depended on the initial bubble size, i.e. smaller bubbles are inherently more unstable to disproportionation due to their higher Laplace pressure. For bubbles of intermediate sizes (~ 350 – 450 μm), the

bubble size was observed to remain almost independent of aging time. The rate of bubble shrinkage via coarsening can be characterized by[53]:

$$R^3(t) = R_0^3 - \left(\frac{t}{\tau}\right) \tag{4}$$

where R(t) and R_o are the bubble radius at time t and t_o, and τ is the coarsening time. Normalizing the bubble coarsening time $\left(\frac{t_i}{t_\infty}\right)$ and bubble size $\left(\frac{b_i}{b_0}\right)$ (where subscript i represents intervals of time, and subscripts 0 and ∞ represent the initial and final measurable conditions), the shrinkage dynamics of the smaller bubbles were in excellent agreement with the bubble shrinkage theory (see Fig. 10c.).
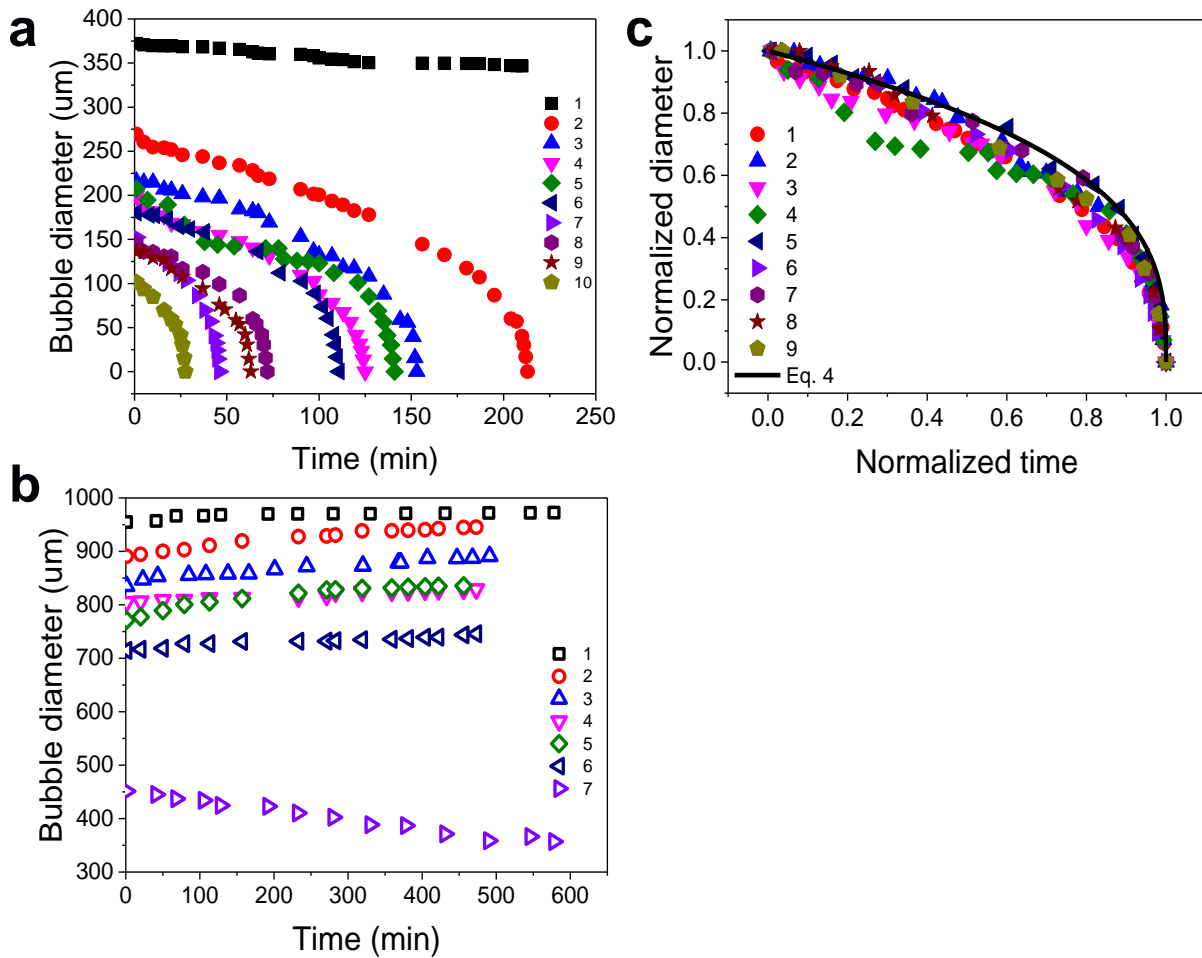
Figure 10. Time-dependent changes in the size of individual bubbles: (a) small bubbles, and (b) large bubbles. (c) Normalized bubble size $(\frac{b_i}{b_0})$ and coarsening time $(\frac{t_i}{t_\infty})$ for nine selected bubbles. Empirical fitting is described by Eq. 4. Foams prepared by dispersing composite particles in 0.55 M Na_2SO_4.

Bubble coarsening was evidenced in all foam systems. While the particle-laden interfaces exhibited mechanical strength they were unable to cease bubble coarsening. Foam coarsening occurs when $\frac{dP}{dR} = -\frac{2\gamma}{R^2} + \frac{4E}{R^2} < 0$,[10] hence bubbles become stable to coarsening when $E > \frac{\gamma}{2}$. From the compressional isotherm data shown in Fig. 3, the compressional elasticity can be calculated from the changes in surface pressure and trough area ($E = -A\frac{d\pi}{dA}$). For all foam systems $E > \frac{\gamma}{2}$ was not satisfied, hence, bubble coarsening contributed to the destabilization of prepared foams. The dynamic compressional elasticity as a function of trough area is shown in Fig. S5 of the Supporting Information.

4. DISCUSSION

Following initial liquid drainage, long-term foam stability becomes a function of the rates of bubble coalescence and coarsening. In the current study, foam stability has been shown to be a function of the electrolyte concentration, with poor foam stability observed at the lowest electrolyte concentration (0.01 M Na_2SO_4), and attributed to a high rate of bubble coalescence due to the increased mobility of the particle-laden layer. Upon bubble-bubble contact the repulsive interaction between neighbouring composite particles facilitates particle migration away from the contact region, resulting in thin liquid film rupture and bubble coalescence. At

higher electrolyte concentrations (0.1 M and 0.55 M Na_2SO_4), the interaction between composite particles was weakly attractive, and we observed the formation of more solid-like particle-laden interfaces of increased rigidity. The interfacial rigidity was partly influenced by the reduced solvation of polymer layers on silica particles with increasing electrolyte concentration. The reduction in solvation will modify the conformation of polymers from an expanded coil when dispersed in pure water (a very good solvent) to a tightly packed globule beyond the theta condition (i.e. poor solvent). Between these two extremes, the coil dimensions will steadily decrease with the reducing solvation of polymer. Evidence for such collapse was seen in the change of particle size shown in Fig. 1. The gradual collapse of the polymer is, in effect moving it from a strongly hydrophilic state towards a more hydrophobic state. This change leads to strengthening of the particle-laden interface, with both a growth of particle aggregates and their increased retention at the air-aqueous interface driven by this decreased solvation of the polymer layers.

Although both particle-laden interfaces prepared using 0.1 M and 0.55 M Na_2SO_4 solutions were elastically dominant (G' > G"), bubble coalescence was observed only in the case of 0.1 M Na_2SO_4 foam. Previous research confirmed that coalescence is feasible when the interfacial shear yield strength of the particle layer is exceeded.[20, 27, 40] In an attempt to understand why bubble coalescence was possible when the particle-laden interfaces were elastically dominant, we considered the relationship between the compressive stress ($P_c = \frac{4\gamma}{R}$) acting on the thin liquid film separating two bubbles intimately in contact,[10] and the yield stress of the particle-laden interface. Assuming an average bubble diameter (2R) of 400 μm and the surface tensions (γ) taken from the data presented in Fig. S3b, the compressive stress exerted on the interacting

34

particle layers was approximately 1.3×10^3 N/m^2 for composite particle foams formed in 0.1 M and 0.55 M electrolyte solutions. Based on the yield points (τ_y) for the two particle layers (0.1 M Na$_2$SO$_4$, $\tau_y = 2.4 \times 10^{-5}$ N/m; 0.55 M Na$_2$SO$_4$, $\tau_y = 5.9 \times 10^{-5}$ N/m), an apparent yield stress can be calculated by introducing a second dimension, which is taken to be the thickness of the interfacial particle layer. Since we did not measure the particle layer thickness, we can reasonably assume that the thickness is equivalent to the hydrodynamic diameter of the composite particles/aggregates. The apparent yield stress (τ'_y) for both the 0.1 M and 0.55 M interfacial particle layers was in the region of 3.0×10^2 N/m^2, and approximately an order of magnitude lower than P_c. Hence, when bubbles are closely packed within a foam, and $P_c \geq \tau'_y$, it is reasonable that the particle-laden interfaces will rupture leading to bridging and bubble coalescence. The absence of bubble-bubble coalescence in foams prepared using composite particles dispersed in 0.55 M Na$_2$SO$_4$ can be attributed to the lack of thin liquid film formation. With strong attraction between composite particles, the resulting large aggregates appear as a network within the continuous aqueous phase, as highlighted by the dashed red box in Fig. 8c. The network impedes liquid drainage therefore inhibiting the formation of thin liquid films between neighboring bubbles (Fig. S4). [48, 49] In the highest electrolyte solution the dominant mechanism for foam collapse was attributed to bubble coarsening.

5. CONCLUSION

A simple method to form polymer-coated silica nanoparticles (composite particles) has been demonstrated, with the stabilizing potential of the composite particles studied as a function of the aqueous electrolyte concentration (Na$_2$SO$_4$). Individually, the two components, polymer and

silica nanoparticles, exhibit no or poor foaming ability. However, with minimal energy input, the composite particles were observed to stabilize foams over several days. Foam lifetimes were shown to increase with increasing electrolyte concentration, and the enhanced foam stability was attributed to the formation of solid-like (armoured) interfacial particle layers surrounding bubbles, with high interfacial layer elasticity resulting from greater particle retention at the air-aqueous interface and strong attraction between neighboring composite particles. The absence of bubble coalescence in foams prepared using 0.55 M Na_2SO_4 was linked to the formation of large particle aggregates, preventing the formation of thin liquid films (plateau borders) between neighboring bubbles. Bubble coarsening was identified to be the dominant foam destabilization mechanism. This study demonstrates the important interplay between species commonly encountered in formulated products, and the synergy between two components to enhance foam stability.

ACKNOWLEDGMENTS

Supporting Information

Thermal Gravimetric Analysis (TGA) for silica nanoparticles, PVP, and composite particles (Fig. S1a); TEM of the composite particles (Fig. S1b); SEM of the silica colloid particle mounted on a tipless silicon nitride AFM cantilever (Fig. S2); droplet contact angle on PVP coated silicon

wafer (Fig. S3a); air-aqueous surface tension measured in the presence of 0.5 wt% PVP and increasing electrolyte concentrations (Fig. S3b); time-dependent liquid volume fractions for foams prepared using 0.1 M and 0.55 M Na_2SO_4 (Fig. S4); compressional elasticity of the 0.01 M, 0.1 M and 0.55 M composite particle layers (Fig. S5); multi-compression π-A isotherms for composite particles deposited at the air-aqueous (0.01 M Na_2SO_4) interface (Fig. S6); optical microscope images of 0.1 M Na_2SO_4 foams taken at 1, 29 and 72 min foam aging (Fig. S7); average bubble size and number of bubbles as a function of foam aging time, electrolyte concentration 0.55 M Na_2SO_4 (Fig. S8).

Corresponding Author

* Email: D.Harbottle@leeds.ac.uk (D.H.)

References

1.　　Hitchcock, J. P.; Tasker, A. L.; Baxter, E. A.; Biggs, S.; Cayre, O. J. Long-Term Retention of Small, Volatile Molecular Species within Metallic Microcapsules. Acs Appl Mater Inter **2015,** 7 (27), 14808-14815.

2.　　Subramaniam, A. B.; Abkarian, M.; Mahadevan, L.; Stone, H. A. Non-spherical bubbles. Nature **2005,** 438 (7070), 930-930.

3.　　Subramaniam, A. B.; Abkarian, M.; Stone, H. A. Controlled assembly of jammed colloidal shells on fluid droplets. Nat Mater **2005,** 4 (7), 553-556.

4.　　Pan, M.; Rosenfeld, L.; Kim, M.; Xu, M. Q.; Lin, E.; Derda, R.; Tang, S. K. Y. Fluorinated Pickering Emulsions Impede Interfacial Transport and Form Rigid Interface for the Growth of Anchorage-Dependent Cells. Acs Appl Mater Inter **2014,** 6 (23), 21446-21453.

5.　　Tan, H.; Sun, G. Q.; Lin, W.; Mu, C. D.; Ngai, T. Gelatin Particle-Stabilized High Internal Phase Emulsions as Nutraceutical Containers. Acs Appl Mater Inter **2014,** 6 (16), 13977-13984.

6.　　Pihan, S. A.; Emmerling, S. G. J.; Butt, H. J.; Berger, R.; Gutmann, J. S. Soft Nanocomposites-From Interface Control to Interphase Formation. Acs Appl Mater Inter **2015,** 7 (23), 12380-12386.

7.   Wang, X. Y.; Feng, X. Y.; Ma, G. P.; Yao, L.; Ge, M. F. Amphiphilic Janus Particles Generated via a Combination of Diffusion-Induced Phase Separation and Magnetically Driven Dewetting and Their Synergistic Self-Assembly. Adv Mater **2016,** 28 (16), 3131-3137.

8.   Binks, B. P. Particles as surfactants - similarities and differences. Curr Opin Colloid In **2002,** 7 (1-2), 21-41.

9.   Rio, E.; Drenckhan, W.; Salonen, A.; Langevin, D. Unusually stable liquid foams. Adv Colloid Interfac **2014,** 205, 74-86.

10.   Martinez, A. C.; Rio, E.; Delon, G.; Saint-Jalmes, A.; Langevin, D.; Binks, B. P. On the origin of the remarkable stability of aqueous foams stabilised by nanoparticles: link with microscopic surface properties. Soft Matter **2008,** 4 (7), 1531-1535.

11.   Maestro, A.; Deshmukh, O. S.; Mugele, F.; Langevin, D. Interfacial Assembly of Surfactant-Decorated Nanoparticles: On the Rheological Description of a Colloidal 2D Glass. Langmuir **2015,** 31 (23), 6289-6297.

12.   Kostakis, T.; Ettelaie, R.; Murray, B. S. Effect of high salt concentrations on the stabilization of bubbles by silica particles. Langmuir **2006,** 22 (3), 1273-1280.

13.   Saigal, T.; Dong, H. C.; Matyjaszewski, K.; Tilton, R. D. Pickering Emulsions Stabilized by Nanoparticles with Thermally Responsive Grafted Polymer Brushes. Langmuir **2010,** 26 (19), 15200-15209.

14.   Alvarez, N. J.; Anna, S. L.; Saigal, T.; Tilton, R. D.; Walker, L. M. Interfacial Dynamics and Rheology of Polymer-Grafted Nanoparticles at Air-Water and Xylene-Water Interfaces. Langmuir **2012,** 28 (21), 8052-8063.

15.   San-Miguel, A.; Behrens, S. H. Influence of Nanoscale Particle Roughness on the Stability of Pickering Emulsions. Langmuir **2012,** 28 (33), 12038-12043.

16.   Briceno-Ahumada, Z.; Langevin, D. On the influence of surfactant on the coarsening of aqueous foams. Adv Colloid Interface Sci **2015**.

17.   Maestro, A.; Rio, E.; Drenckhan, W.; Langevin, D.; Salonen, A. Foams stabilised by mixtures of nanoparticles and oppositely charged surfactants: relationship between bubble shrinkage and foam coarsening. Soft Matter **2014,** 10 (36), 6975-6983.

18.   Maestro, A.; Guzman, E.; Santini, E.; Ravera, F.; Liggieri, L.; Ortega, F.; Rubio, R. G. Wettability of silica nanoparticle-surfactant nanocomposite interfacial layers. Soft Matter **2012,** 8 (3), 837-843.

19.   Erni, P.; Jerri, H. A.; Wong, K.; Parker, A. Interfacial viscoelasticity controls buckling, wrinkling and arrest in emulsion drops undergoing mass transfer. Soft Matter **2012,** 8 (26), 6958-6967.

20.   Harbottle, D.; Chen, Q.; Moorthy, K.; Wang, L. X.; Xu, S. M.; Liu, Q. X.; Sjoblom, J.; Xu, Z. H. Problematic Stabilizing Films in Petroleum Emulsions: Shear Rheological Response of Viscoelastic Asphaltene Films and the Effect on Drop Coalescence. Langmuir **2014,** 30 (23), 6730-6738.

21.   Bolten, D.; Turk, M. Experimental Study on the Surface Tension, Density, and Viscosity of Aqueous Poly(vinylpyrrolidone) Solutions. J Chem Eng Data **2011,** 56 (3), 582-588.

22.   Folmer, B. M.; Kronberg, B. Effect of surfactant-polymer association on the stabilities of foams and thin films: Sodium dodecyl sulfate and poly(vinyl pyrrolidone). Langmuir **2000,** 16 (14), 5987-5992.

23.   von Klitzing, R.; Muller, H. J. Film stability control. Curr Opin Colloid In **2002,** 7 (1-2), 42-49.

24.   Guerrini, R. M.; Lochhead, R. Y.; Daly, W. H. Interactions of aminoalkylcarbamoyl cellulose derivatives and sodium dodecyl sulfate. 2. Foam stabilization. Colloid Surface A **1999,** 147 (1-2), 67-78.

25.   Pinaud, F.; Geisel, K.; Masse, P.; Catargi, B.; Isa, L.; Richtering, W.; Ravaine, V.; Schmitt, V. Adsorption of microgels at an oil-water interface: correlation between packing and 2D elasticity. Soft Matter **2014,** 10 (36), 6963-6974.

26.   Geisel, K.; Isa, L.; Richtering, W. Unraveling the 3D Localization and Deformation of Responsive Microgels at Oil/Water Interfaces: A Step Forward in Understanding Soft Emulsion Stabilizers. Langmuir **2012,** 28 (45), 15770-15776.

27.   Li, Z. F.; Harbottle, D.; Pensini, E.; Ngai, T.; Richtering, W.; Xu, Z. H. Fundamental Study of Emulsions Stabilized by Soft and Rigid Particles. Langmuir **2015,** 31 (23), 6282-6288.

28.   Niskanen, J.; Wu, C.; Ostrowski, M.; Fuller, G. G.; Hietala, S.; Tenhu, H. Thermoresponsiveness of PDMAEMA. Electrostatic and Stereochemical Effects. Macromolecules **2013,** 46 (6), 2331-2340.

29.   Nazli, K. O.; Pester, C. W.; Konradi, A.; Boker, A.; van Rijn, P. Cross-Linking Density and Temperature Effects on the Self-Assembly of SiO2-PNIPAAm Core-Shell Particles at Interfaces. Chem-Eur J **2013,** 19 (18), 5586-5594.

30.   Ullrich, S.; Scheeler, S. P.; Pacholski, C.; Spatz, J. P.; Kudera, S. Formation of Large 2D Arrays of Shape-Controlled Colloidal Nanoparticles at Variable Interparticle Distances. Part Part Syst Char **2013,** 30 (1), 102-108.

31.   Isa, L.; Calzolari, D. C. E.; Pontoni, D.; Gillich, T.; Nelson, A.; Zirbs, R.; Sanchez-Ferrer, A.; Mezzenga, R.; Reimhult, E. Core-shell nanoparticle monolayers at planar liquid-liquid interfaces: effects of polymer architecture on the interface microstructure. Soft Matter **2013,** 9 (14), 3789-3797.

32.   Geisel, K.; Rudov, A. A.; Potemkin, I. I.; Richtering, W. Hollow and Core-Shell Microgels at Oil-Water Interfaces: Spreading of Soft Particles Reduces the Compressibility of the Monolayer. Langmuir **2015,** 31 (48), 13145-13154.

33.   Robinson, S.; Williams, P. A. Inhibition of protein adsorption onto silica by polyvinylpyrrolidone. Langmuir **2002,** 18 (23), 8743-8748.

34.   McFarlane, N. L.; Wagner, N. J.; Kaler, E. W.; Lynch, M. L. Poly(ethylene oxide) (PEO) and Poly(vinyl pyrolidone) (PVP) Induce Different Changes in the Colloid Stability of Nanoparticles. Langmuir **2010,** 26 (17), 13823-13830.

35.   Pattanaik, M.; Bhaumik, S. K. Adsorption behaviour of polyvinyl pyrrolidone on oxide surfaces. Mater Lett **2000,** 44 (6), 352-360.

36.   Koczkur, K. M.; Mourdikoudis, S.; Polavarapu, L.; Skrabalak, S. E. Polyvinylpyrrolidone (PVP) in nanoparticle synthesis. Dalton T **2015,** 44 (41), 17883-17905.

37.   McNamee, C. E., Yamamoto, S., Butt, H., Higashitani, K. A Straightforward Way To Form Close-Packed TiO$_2$ Particle Monolayers at an Air/Water Interface. Langmuir **2010,** 27, 887–894.

38.   Vandebril, S.; Franck, A.; Fuller, G. G.; Moldenaers, P.; Vermant, J. A double wall-ring geometry for interfacial shear rheometry. Rheol Acta **2010,** 49 (2), 131-144.

39.   Goodwin, D. J.; Sepassi, S.; King, S. M.; Holland, S. J.; Martini, L. G.; Lawrence, M. J. Characterization of Polymer Adsorption onto Drug Nanoparticles Using Depletion Measurements and Small-Angle Neutron Scattering. Mol Pharmaceut **2013,** 10 (11), 4146-4158.

40.   Zhang, H.; Yu, K.; Cayre, O. J.; Harbottle, D. Interfacial Particle Dynamics: One and Two Step Yielding in Colloidal Glass. Langmuir **2016,** 32 (50), 13472-13481.

41.   Hunter, T. N.; Pugh, R. J.; Franks, G. V.; Jameson, G. J. The role of particles in stabilising foams and emulsions. Adv Colloid Interfac **2008,** 137 (2), 57-81.

42.   Razavi, S. C., K. D.; Lin, B.; Lee, K. Y. C.; Tu, R. S.; Kretzschmar, I. Collapse of Particle-Laden Interfaces under Compression: Buckling vs Particle Expulsion. Langmuir **2015,** 31, 7764−7775.

43.   Noskov, B. A.; Akentiev, A. V.; Loglio, G.; Miller, R. Dynamic surface properties of solutions of poly(ethylene oxide) and polyethylene glycols. J Phys Chem B **2000,** 104 (33), 7923-7931.

44.   Noskov, B. A.; Akentiev, A. V.; Miller, R. Dynamic surface properties of poly(vinylpyrrolidone) solutions. J Colloid Interf Sci **2002,** 255 (2), 417-424.

45.   Saint-Jalmes, A.; Langevin, D. Time evolution of aqueous foams: drainage and coarsening. J Phys-Condens Mat **2002,** 14 (40), 9397-9412.

46.   Hackbarth, J. J. Multivariate analyses of beer foam stand. J I Brewing **2006,** 112 (1), 17-24.

47.   Dale, C.; West, C.; Eade, J.; Rito-Palomares, M.; Lyddiatt, N. Studies on the physical and compositional changes in collapsing beer foam. Chem Eng J **1999,** 72 (1), 83-89.

48.   Carn, F.; Colin, A.; Pitois, O.; Vignes-Adler, M.; Backov, R. Foam Drainage in the Presence of Nanoparticle-Surfactant Mixtures. Langmuir **2009,** 25 (14), 7847-7856.

49.   Haffner, B.; Khidas, Y.; Pitois, O. Flow and jamming of granular suspensions in foams. Soft Matter **2014,** 10 (18), 3277-3283.

50.   Bhamla, M. S.; Giacomin, C. E.; Balemans, C.; Fuller, G. G. Influence of interfacial rheology on drainage from curved surfaces. Soft Matter **2014,** 10 (36), 6917-6925.

51.   Israelachvili, J. N. Intermolecular and Surface Forces; Third ed.; Elsevier: USA, 2011.

52.   Natarajan, A.; Kuznicki, N.; Harbottle, D.; Masliyah, J.; Zeng, H.; Xu, Z. Molecular Interactions between a Biodegradable Demulsifier and Asphaltenes in an Organic Solvent. Energy & Fuels **2016**.

53.   Dickinson, E.; Ettelaie, R.; Kostakis, T.; Murray, B. S. Factors controlling the formation and stability of air bubbles stabilized by partially hydrophobic silica nanoparticles. Langmuir **2004,** 20 (20), 8517-8525.